Cell Communication and Signaling

RESEARCH

Open Access

ONC212, alone or in synergistic conjunction with Navitoclax (ABT-263), promotes cancer cell apoptosis via unconventional mitochondrial-independent caspase-3 activation

Vishal Basu[1†], Shabnam[1†], Yamini Murghai[1], Maqsood Ali[1], Swetangini Sahu[1], Bhupendra K. Verma[1] and Mahendra Seervi[1*]

Abstract

Mitochondria-targeting agents, known as mitocans, are emerging as potent cancer therapeutics due to pronounced metabolic and apoptotic adaptations in the mitochondria of cancer cells. ONC212, an imipridone-family compound initially identified as a ClpP agonist, is currently under investigation as a potential mitocan with demonstrated preclinical efficacy against multiple malignancies. Despite this efficacy, the molecular mechanism underlying the cell death induced by ONC212 remains unclear. This study systematically investigates the mitochondrial involvement and signaling cascades associated with ONC212-induced cell death, utilizing HeLa and A549 cancer cells. Treated cancer cells exhibited characteristic apoptotic features, such as annexin-V positivity and caspase-3 activation; however, these occurred independently of typical mitochondrial events like membrane potential loss ($\Delta\Psi_m$) and cytochrome c release, as well as caspase-8 activation associated with the extrinsic pathway. Additionally, ONC212 treatment increased the expression of anti-apoptotic proteins Bcl-2 and Bcl-xL, which impeded apoptosis, as the overexpression of Bcl-2-GFP and Bcl-xL-GFP significantly reduced ONC212-mediated cell death. Furthermore, combining a sub-lethal dose of the Bcl-2/Bcl-xL inhibitor Navitoclax with ONC212 markedly augmented caspase-3 activation and cell death, still without any notable $\Delta\Psi_m$ loss or cytochrome c release. Moreover, inhibition of caspase-9 activity unexpectedly augmented, rather than attenuated, caspase-3 activation and the subsequent cell death. Collectively, our research identifies ONC212 as an atypical mitochondrial-independent, yet Bcl-2/Bcl-xL-inhibitable, caspase-3-mediated apoptotic cell death inducer, highlighting its potential for combination therapies in tumors with defective mitochondrial apoptotic signaling.

Keywords ONC212, Mitochondria, Cell death, Navitoclax, Apoptosis, Caspase-3, Bcl-2

Introduction

Ever since the 'Warburg effect' [1] was discovered, mounting evidence has unequivocally established the vital role of mitochondria in cancer. The altered bioenergetic state and defective apoptotic machinery are the crucial hallmarks of cancer, both of which are directly governed by mitochondria [2, 3]. Given this differential

†Vishal Basu and Shabnam[1] contributed equally to this work.

*Correspondence:
Mahendra Seervi
mseervi.bt@aiims.edu
[1] Department of Biotechnology, All India Institute of Medical Sciences (AIIMS), New Delhi 110029, India

state of mitochondria in cancer cells, mitochondria have emerged as an intriguing pharmacological target in cancer therapy. Recently proposed 'mitocans' are the agents that act directly on mitochondria and hold promise for the development of potential anticancer drugs owing to their selectivity for cancer cells [4–6]. The last two decades witnessed an unprecedented focus on the discovery of novel mitocans.

Among mitocans, the imipridone family has lately emerged as a prospective cancer therapeutic. When compared to other mitocan families, drugs of the imipridone family have a similar tri-heterocyclic core chemical structure but unique peripheral moieties [7–9]. The lead molecule in the family, ONC201, is already undergoing phase 2 clinical trials for solid tumors and hematologic malignancies [10]. However, attention has recently shifted to its derivative ONC212 (TR-31), given its demonstrated broad-spectrum anticancer efficacy against various in vitro and in vivo models of malignancies such as pancreatic, breast, glioblastoma, etc. [10–15]. In addition to its effectiveness as a standalone treatment, ONC212 displayed notable synergistic potential when paired with a range of chemotherapeutic drugs in various cancer cell lines [14, 15]. Although various studies have highlighted divergent molecular targets of ONC201 and ONC212, the underlying death mechanism still remains obscure.

ONC201 was initially discovered as a TRAIL/DR5-inducing compound capable of eliciting extrinsic apoptosis and growth arrest via the integrated stress response [16–18]. Subsequently, the plasma membrane protein GPCR GPR132 was identified as a novel target of ONC212 in hematologic cancers. GPCR GPR132 targeting promotes Gq signaling, which leads to death in cancer cells by activating transcription factors ATF4 and CHOP. [14].

More recently, the mitochondrial peptidase ClpP has been identified as an intracellular target of both ONC201 and ONC212 in hematologic malignancies [19–22]. ClpP is a double-ringed tetradecameric oligomeric serine protease with a hollow chamber ClpX that contains proteolytic active sites. ClpX recognizes and unfolds native substrates in an ATP-dependent manner and introduces them into the ClpP protease barrel for degradation. These complexes are essential for maintaining mitochondrial protein homeostasis and cellular bioenergetics [19, 20]. Mechanistically, ONC212 promotes hyperactivation of ClpP, which causes ClpX to dissociate from the complex, resulting in proteolysis of respiratory chain proteins. Proteolysis impairs oxidative phosphorylation (OXPHOS) and ATP flux, disrupting mitochondrial function and cause selective cancer cell death, regardless of p53 status [12, 13]. Interestingly, since ONC212 targets oxidative metabolism, it specifically targeted breast cancer stem cells (CSCs), as CSCs are highly dependent on OXPHOS and mitochondrial activity, whereas cancer cells that rely on glycolysis experience growth arrest [23–25]. The CSCs are a distinct subset of tumor-initiating cells that may self-renew and hence contribute to tumor initiation, progression and heterogeneity [26]. All these evidences highlighted ONC212 as a novel mitocan with the potential anticancer activity that may have clinical utility in cancer therapy either as a single agent or in combination with other drugs.

Although various extracellular and intracellular molecular targets of ONC212 have been highlighted in the previous reports, the mechanism by which these molecules trigger a downstream apoptotic signaling cascade has not yet been explored. Moreover, despite the emerging therapeutic interest of ONC212 as a mitocan, the crucial mitochondrial apoptotic events are yet to be identified. Since most cancer cells have defective apoptotic machinery, the systematic and comprehensive understanding of the cell death signaling triggered by ONC212 may lead to its better utility and implication as cancer therapeutics. Our aim was therefore to unravel the ONC212-induced apoptotic signaling cascade employing different cancer cell lines.

Materials and methods

Cell lines and maintenance

HeLa (Cervical cancer) and A549 (Lung carcinoma) cell lines were procured from the National Centre for Cell Science (NCCS), India. All cells were maintained in Dulbecco's Modified Eagle's Medium (HiMedia, India) supplemented with 10% heat-inactivated Fetal Bovine Serum (GIBCO, USA) and 1X antibiotic antimycotic cocktail (GIBCO, USA) in a humified incubator with 5% CO_2.

Reagents, plasmids and antibodies

The compounds ONC212, Navitoclax (ABT-263) and Tanespimycin (17-AAG) were obtained from MedChemExpress (NJ, USA) while Etoposide was obtained from Sigma-Aldrich (Missouri, USA). Pan-caspase inhibitor (Z-VAD-FMK) and caspase-9 inhibitor III (Ac-LEHD-CMK) were purchased from (Santa Cruz Biotechnology, USA).

Bcl-2-GFP and Bcl-xL-GFP plasmids were kindly gifted by Dr. Clark W. Distelhorst (Case Western Reserve University, Cleveland, Ohio). Caspase-3 sensor plasmid pCDH-puro-CMV-GC3AI was procured from Addgene (MA, USA).

Antibodies: GAPDH and β-Actin (Proteintech, USA); cleaved caspase-3 (Asp175), cleaved caspase-9 (Asp330), caspase-8 (1C12), PARP-1(46D11), Bax (D2E11), Bak (D4E4), Bcl-xL, Bcl-2, TRAP-1, EMT antibody sampler

kit (Cell Signaling Technology, USA); Cytochrome-c (6H2) (Santa Cruz Biotechnologies, USA).

Generation of stable cell lines

Bcl-2 GFP and Bcl-xL GFP stable cell lines were generated as previously described in [27]. Briefly, the plasmid was transfected in cells using Lipofectamine™ LTX plus (Thermo Fisher Scientific, USA) as per the standard protocol. Cells were maintained in selection media containing G418 antibiotic (Thermo Fisher Scientific, USA) for a week and then, GFP-positive cells were sorted via flow cytometry (BD, FACSAria™ Fusion).

HeLa cytochrome c -GFP cells were a kind gift from Dr. T. R. Santhosh Kumar (Rajiv Gandhi Centre for Biotechnology, Kerala, India).

Cell cytotoxicity assay

To assess the cell viability, an MTT assay was performed as per standard protocol. Briefly, cells were seeded in 96 well plates and treated with various concentrations of test agent. Post-treatment, MTT solution was added and incubated for 3 h at 37 °C. The solvent was added to dissolve the formazan crystal and after 30 min, absorbance was measured at 590 nm.

Assays for the analysis of cell death

Annexin V-FITC/PI staining assay

Annexin V-FITC/PI apoptosis detection kit (Thermo Fisher Scientific, USA) was used to assess different stages of apoptosis as per the manufacture's standard protocol. Briefly, following trypsinization, cells were washed using 1X PBS and stained with Annexin V at a dilution of 1:50 in 1X Annexin V binding buffer for 30 min at 37 °C, along with a 2 µg/ml Propidium iodide (PI) stain. Subsequently, the stained cells were diluted in 300 µl of 1X annexin binding buffer and subjected to flow cytometry (BD, FACSymphony™) for fluorescence analysis.

Zombie™ dye staining assay

Alternatively, Zombie™ dye (BioLegend, San Diego, CA) was employed to assess live and dead cells according to the manufacturer's protocol. Cells grown and treated in 24 well plate were harvested, washed with 1X PBS and stained with Zombie™ dye at a 1:800 dilution in PBS for 30 min at room temperature in the dark. The stained cells were then diluted in 200 µl of 1X PBS and examined using flow cytometry (BD, FACSymphony™) utilizing the PE channel.

Nuclei condensation

Treated and untreated cells were stained with 0.5 µg/ml of the nuclear stain Hoechst 33,342 (Sigma, MO, USA) for 10 min. The stained cells were imaged with UV-filter of Nikon Ti-U inverted fluorescent microscope (Tokyo, Japan) equipped with NIS imaging software. Cells with apoptotic condensed nuclei were scored as percentage per sample and for each assay, and three random fields were scored.

Assessment of intracellular caspase-3 activity

For assessing the intracellular activity of activated caspase-3, the Caspase 3/7 Assay Kit (Magic Red, Abcam) was used, according to the manufacturer's protocol. The stock staining solution was prepared by dissolving MR-(DEVD)2 in DMSO and subsequently diluting (1/5th) in diH_2O for the working solution. Cells grown in 24 well plates were harvested and then, stained with 300 µl of staining solution with periodic swirls at 37 °C for 60 min in the dark and subjected to flow cytometric analysis.

In addition, cells with transiently expressing caspase-3 sensor GC3AI plasmid were seeded in a 24 well plate. After treatment with test agent, cells were harvested and fluorescence intensity was measured using flow cytometry's FITC channel.

Immunofluorescence

Cells were cultured on polymer-coated coverslip 8-well chamber slides (Lab-Tek™ II chamber slides (Thermo Fisher Scientific, USA) and incubated with specific drugs for defined periods. Post-incubation, cells were rinsed with 1X PBS and subsequently fixed with 4% paraformaldehyde solution in 1X PBS for 12 min at room temperature. Afterward, cells were kept in an immunofluorescence buffer (1X PBS, 10 mg/mL BSA, 0.02% SDS, and 0.1% Triton X-100) for 2 h. Subsequently, the cells were incubated overnight at 4 °C with the primary antibody diluted in the immunofluorescence buffer followed by incubation with Alexa Fluor 488 tagged secondary antibody (Abcam) for 2 h. Finally, the cells were rinsed thrice with the immunofluorescence buffer, and nuclei were counterstained with DAPI. Coverslips were mounted with Prolong™ Diamond mounting media (Life Technologies) and fluorescent images were acquired utilizing a NIKON confocal microscope with a 60X oil immersion objective. The obtained images were processed using FIJI software for further analysis and presentation.

Analysis of mitochondrial membrane potential ($\Delta\Psi_m$)

To analyse mitochondrial transmembrane potential ($\Delta\Psi_m$), cells were stained with 25 nM TMRM dye (Molecular Probes, USA) and relative fluorescence was evaluated either using flow cytometry or fluorescent microscopy as per the previously described method [27].

As an alternative method, cells were stained with JC1 (Molecular probes, USA) and incubated for 20 min

before capturing images under fluorescent microscope to detect JC1 aggregates (Ex/Em = 540/590 nm) and monomeric forms (Ex/Em = 485/535 nm).

Cell cycle analysis

Cell cycle stages were determined by PI staining, followed by flow cytometric analysis as per the standard protocol. Briefly, cells grown in 12 well plates were harvested and fixed in pre-cold 70% ethanol for 45 min on ice. Cells were rinsed with 1X PBS and RNase (100 µg/ml) was added to the samples. The cell pellet was stained with 10 µg/ml PI staining solution (Thermo Fisher Scientific, USA) and incubated in the dark at room temperature for 30 min before analyzed by flow cytometry.

Western blotting

Standard protocol was followed for western blot as previously described [28].

Western blot densitometric quantification: Western blots were analysed using ImageJ software (NIH, USA). Band intensities were measured using the gel analysis tool. Each protein of interest was normalized to its corresponding loading control (e.g., β-actin). Normalized values were expressed as fold change relative to control samples. Quantification was performed on two independent experiments.

Clonogenicity assay

Post treatment, cells were trypsinized, serially diluted at a 1:100 ratio, and reseeded into a new 12-well plate with a very low cell population (100–200). These cells were maintained for 20–25 days to visualize the colony formation. Subsequently, cells were fixed with pre-chilled acetone: methanol (1:1) solution, stained with 0.5% crystal violet solution for 45 min and rinsed thrice with 1X PBS. For colorimetric quantification, the crystal violet stain of the control and test well was dissolved in an equal volume of DMSO and absorbance was measured at 590 nm. Relative clonogenicity was calculated by multiplying the absorbance of the test well by 100 and dividing it by the absorbance of the untreated well.

Statistical analysis

The data are expressed as the mean or standard deviation. GraphPad Prism 8.0 was used for all the statistical analyses. Student's t test was used for comparisons between two groups. One-way ANOVA was used to compare the means of three or more groups with one independent variable. Significance was designated as follows: $^{*}p < 0.05$, $^{**}p < 0.01$, $^{***}\ p < 0.001$. P values are indicated in the figures, and $P < 0.05$ was considered significant.

Results

ONC212 induces permanent cell cycle arrest and apoptosis

To assess the cytotoxic effect of ONC212 in different cancer cells, MTT assay was performed in HeLa and A549, the widely used human cervical and lung alveolar cancer cell lines respectively. As illustrated in Fig. 1a and b, incubation with ONC212 for 48 h significantly reduced the number of viable cells in both cell lines in a dose-dependent manner. The IC_{50} value for ONC212 in HeLa and A549 cells was determined using the MTT assay to be 16 µM and 54 µM, respectively. For subsequent study, we have used 15 µM and 50 µM dose of ONC212 for HeLa and A549 cells respectively. Morphological study using bright field microscopy revealed significant cell death in both cells at these doses (Fig. S1a and b). Nuclear condensation and annexin V/PI assays were performed to assess apoptotic cell death in both control cancer cells and ONC212-treated HeLa and A549 cells for 48 h [29–31]. As shown in Fig. 1c and d, chromatin condensation was observed significantly at 48 h in the ONC212-treated cells indicating the occurrence of apoptosis whereas the nuclear morphology was intact and normal in the control cells. Subsequently, annexin-V/PI assay in both HeLa and A549 cancer cells revealed significant increases in apoptotic cell populations following 48 h of ONC212 treatment compared to untreated cells. Representative flow cytometry scatter plots clearly illustrate this shift, with ONC212-treated cells showing markedly higher proportions in the early and late apoptotic quadrants i.e., Q4 and Q2 respectively (Fig. 1e and f). Quantitative analysis of these data, presented as bar graphs, demonstrates a statistically significant increase in the percentage of total

(See figure on next page.)

Fig. 1 ONC212 induce apoptotic cell death in HeLa and A549 cancer cells. **a.** The viability of HeLa was determined by MTT assay at different concentrations (5 to 20 µM) of ONC212 treatment for 48 h. The IC_{50} value was calculated to be 16.3 µM. **b.** A549 cell viability was assessed by MTT assay with ONC212 exposure (20 to 60 µM) for 48 h. The IC_{50} value was determined to be 54 µM. **c.** Hoechst-stained pictures of ONC212-induced nuclear condensation (20X objective, scale bar: 50 µm). Condensed nuclei are indicated by arrows. **d.** Percentage of condensed nuclei in random fields represented graphically ($n = 3$, mean ± SEM), **denotes $p < 0.01$ in control *vs* ONC212 treated cells (48 h). **e** & **f.** Representative flow cytometry scatter plots of Annexin-V FITC/PI staining in control and ONC212-treated cells. ONC212 treatment increased the proportion of early and late apoptotic cell populations compared to untreated control. **g.** Quantification of total apoptotic cells (Annexin V-positive, with or without PI positivity) expressed as a percentage of the total cell population. ($n = 2$, mean ± SEM), ** denotes $p < 0.01$ and *** denotes $p < 0.001$ in control vs ONC212 treated cells (48 h). **h** & **i.** Clonogenicity assay showing the survival efficacy of cancer cells after ONC212 treatment for 48 h. Cell density (displayed by crystal violet staining) was effectively reduced in ONC212-treated cancer cells than untreated control. Percentage of clonogenicity is assessed by colorimetric analysis of crystal violet staining and represented graphically ($n = 3$, mean ± SEM and **denotes $p < 0.01$) in both untreated vs treated

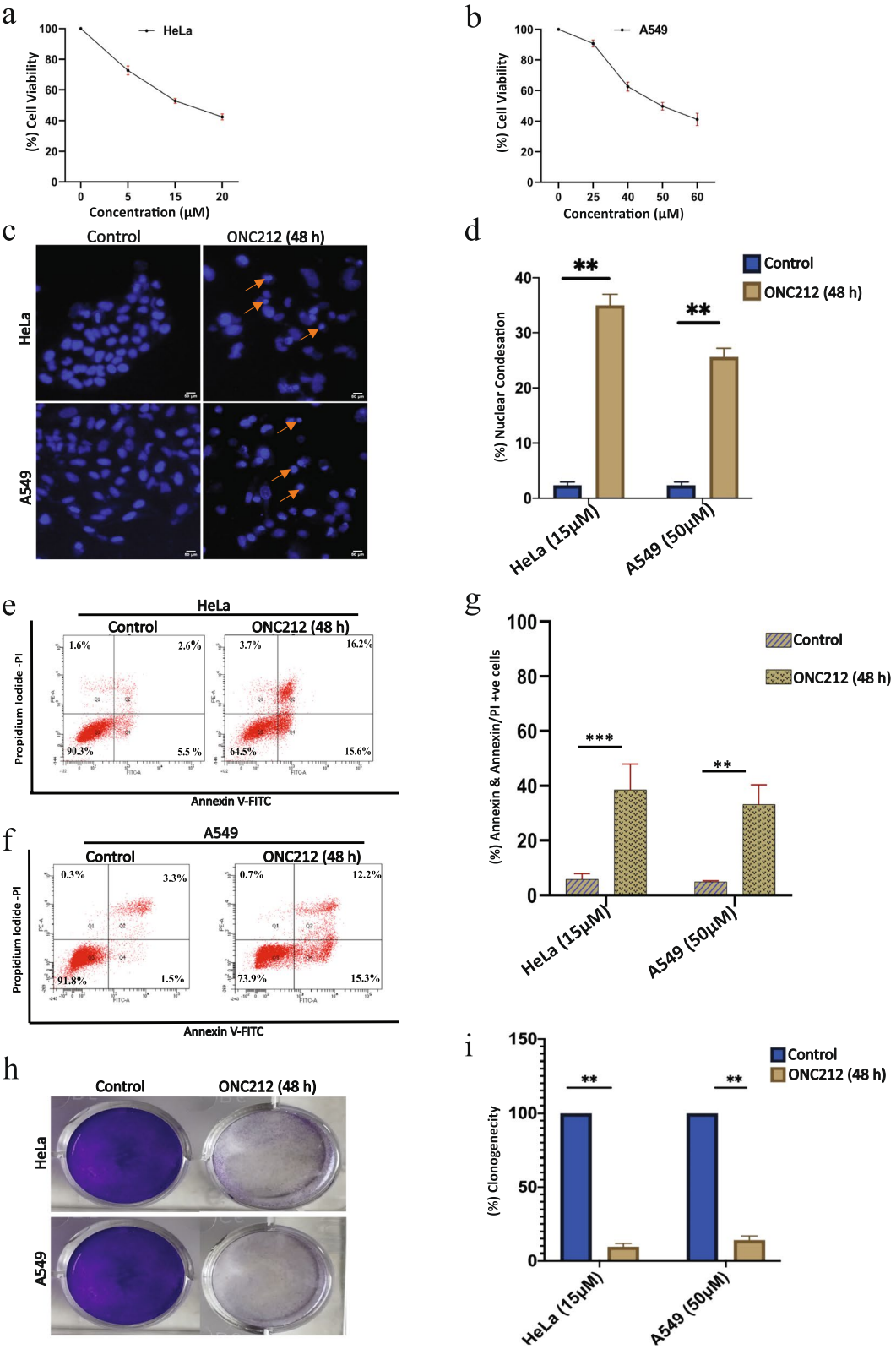

Fig. 1 (See legend on previous page.)

apoptotic cells (Annexin V-positive, with or without PI positivity) in ONC212-treated samples compared to controls (Fig. 1g).

As most anti-cancer drugs cause cell cycle arrest prior to cell death [31–33], we analyzed cell cycle stages in control and ONC212-treated cancer cells by PI staining followed by flow cytometric analysis. As shown in Fig. S2a and b, ONC212 treatment (24 h) led to a significant accumulation of cells at G1/G0 phase in both the cancer cells. This suggests that ONC212-induced cell cycle arrest at the G1/G0 phase before inducing apoptotic cell death. A clonogenicity assay was performed to further

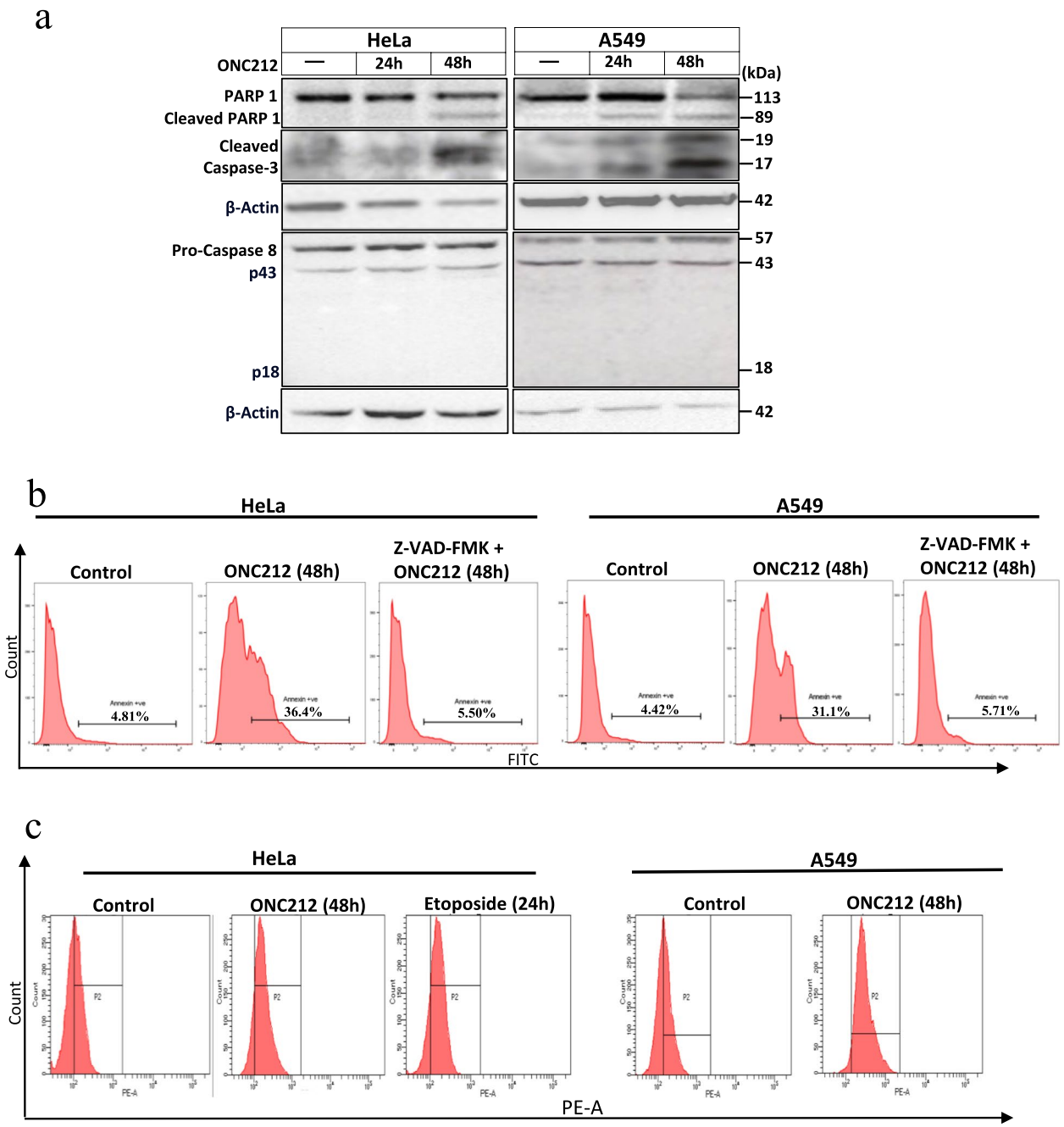

Fig. 2 ONC212 induced caspase-dependent apoptosis in cancer cells. **a.** The western blot demonstrated that ONC212 treatment gradually (24 h and 48 h) induced effective caspase-3 and PARP cleavage in both HeLa and A549 cancer cells. Caspase-8 cleavage did not occur upon ONC212 treatment. **b**. Flow cytometry histograms comparing apoptotic cell death via annexin-V-FITC staining assay in ONC212 treated HeLa and A549 cells for 48 h in the presence and absence of pan-caspase inhibitor (Z-VAD-FMK). **c.** Flow cytometry histogram plots showing ONC212-induced caspase-3,7 activity assessed by caspase 3/7 Magic Red staining of HeLa and A549 cancer cells. Etoposide (20 μM, 24 h) was used as the positive control. The shifting of the ONC212-treated cell population towards the right-side suggests enhanced caspase-3,7 activity

investigate the reproductive viability of ONC212-treated cancer cells. Interestingly, ONC212-treated cancer cells failed to form colonies for almost 20 days whereas untreated cancer cells became confluent in the meantime (Fig. 1h and i). These findings substantiate that ONC212 caused persistent cell cycle arrest in both HeLa and A549 cell lines, as well as a decrease in proliferative capacity.

ONC212 triggers caspase-3 mediated apoptosis

In both intrinsic and extrinsic pathways of apoptosis, the death signal ultimately leads to cleavage and activation of caspase-3 [31, 34]. Caspase-3 activation represents the executioner phase of apoptosis in which the death signal is propagated via proteolytic enzymatic activity on its substrate proteins [35]. Therefore, for further validation of apoptosis, we assessed the caspase-3 cleavage in ONC212-treated cancer cells. As illustrated by western blot (Fig. 2a and S2c), ONC212 treatment for 24 h revealed a minor caspase-3 cleavage, which was further enhanced at 48 h of treatment in both HeLa and A549 cells. Similarly, we also observed significant cleavage of PARP-1 [36], a well-known substrate of activated caspase-3 in ONC212-treated cells at 48 h.

Principally, the activation of initiator caspase-8 or caspase-9 results in the subsequent activation of caspase-3 in the extrinsic or intrinsic apoptotic signaling pathways, respectively [31, 37]. However, we did not observe any caspase-8 cleavage in ONC212-treated cancer cells compared to untreated cells (Fig. 2a and S2c). Hence, it can be inferred that ONC212 induces caspase-3 activation in a caspase-8 independent manner, thereby excluding the possibility of ONC212 treatment inducing the death receptor/extrinsic pathway.

To investigate whether ONC212 elicits caspase-dependent cell death, we analyzed cell death in A549 and HeLa cancer cell lines treated with ONC212 alone or in combination with the pan-caspase inhibitor Z-VAD-FMK for 48 h. Flow cytometry analysis of Annexin-V-FITC staining (Fig. 2b) and Zombie Red staining (Fig. S2d) showed that Z-VAD-FMK significantly reduced ONC212-induced cell death, as evidenced by decreased Annexin-V-positive and Zombie Red-positive populations. These results indicate a primary role for caspase-dependent apoptosis in ONC212-mediated cytotoxicity.

To further verify and quantify caspase-3 activity, cells were stained with fluorogenic caspase-3 substrate followed by flow cytometric analysis. ONC212-treated HeLa cancer cells showed potent caspase-3 activity at 48 h, comparable to positive control Etoposide treatment (20 μM, 24 h), as seen by the enhanced fluorescence intensity in whole cancer cell population compared to untreated cells (Fig. 2c). Similarly, caspase-3 activity was also observed in ONC212-treated A549 cancer cells (Fig. 2c). These results clearly corroborate that ONC212 triggers executioner caspase-3 cleavage and activation in both HeLa and A549 cancer cells which leads to apoptotic cell death.

ONC212 induces apoptosis without mitochondrial membrane potential ($\Delta\Psi_m$) loss and cytochrome c release

Since ONC212 has previously been reported as the potential mitocan [11], we anticipated that ONC212 might be triggering caspase-3 activity via induction of the intrinsic/mitochondrial pathway of apoptosis. Primarily, in this process, mitochondrial outer membrane permeabilization (MOMP) causes the cytochrome c (cyt-c) protein from the intermembrane space to be released into the cytosol [38, 39]. Consequently, this leads to the activation of initiator caspase-9 through the formation of the apoptosome protein complex. To clarify the involvement of mitochondria in ONC212-mediated apoptosis, we initially assessed the $\Delta\Psi_m$ by staining the cells with TMRM dye, followed by flow cytometric analysis. $\Delta\Psi_m$ loss implies a reduction in the fluorescence intensity of TMRM dye [29, 38]. Surprisingly, there was no significant reduction in the fluorescence intensity of TMRM in ONC212-treated HeLa and A549 cancer cells at 48 h compared to control cells, as shown in Fig. 3a. Whereas, as the positive control, etoposide treatment caused distinctive reduction in the TMRM fluorescence intensity in HeLa cells when compared to untreated cells (shown in Fig. 6a). To further substantiate this observation, we performed cell staining with another $\Delta\Psi_m$ probe, a cyanine dye JC-1 and observed the cells under fluorescence

(See figure on next page.)

Fig. 3 ONC212 failed to induce mitochondrial membrane potential ($\Delta\Psi_m$) loss and cytochrome c release. **a.** Flow cytometry histogram showing the relative fluorescence intensity of mitochondrial stain TMRM in ONC212-treated (24 h, 48 h) compared to untreated HeLa and A549 cancer cells. Insignificant reduction in TMRM intensity suggests unaltered $\Delta\Psi_m$ in cells exposed to ONC212. **b.** Fluorescent microscopic images of cells stained simultaneously with TMRM and Hoechst 33,342 (20X, scale bar: 50 μm). TMRM intensity was not reduced significantly upon ONC212 treatment. However, out of total condensed nuclei, very few nuclei with massive condensation showed loss of TMRM stain. **c.** Cytochrome c release from mitochondria was assessed by immunofluorescence and representative images are shown for control and ONC212-treated HeLa (40X, scale bar: 50 μm and A549 (60X, scale bar: 50 μm) cancer cells. Notably, cells with condensed nuclei (DAPI stain) did not reveal a diffuse (cytosolic) pattern of cyt-c but rather a predominantly granular (mitochondrial) pattern

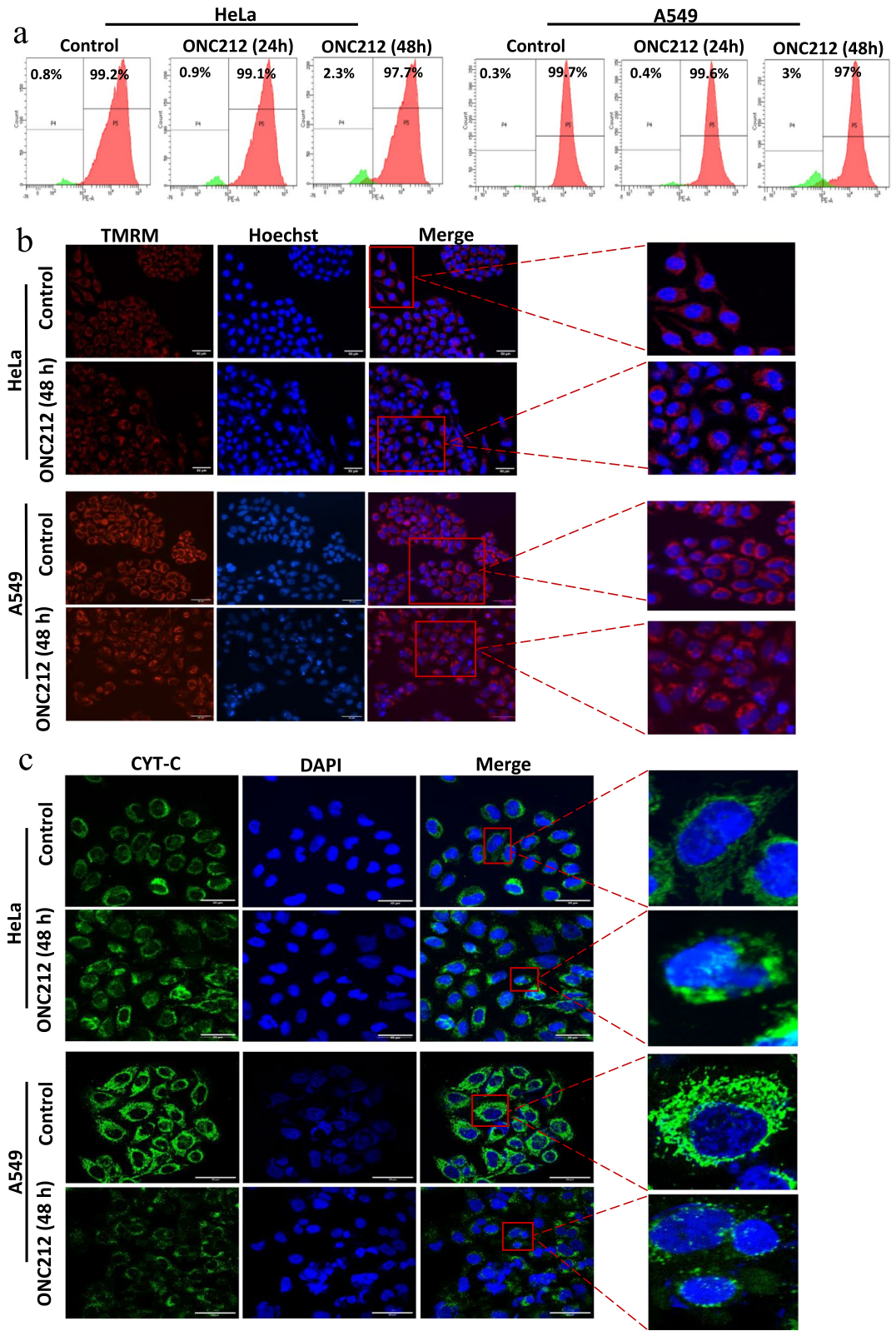

Fig. 3 (See legend on previous page.)

microscope. The results show a negligible shift from red to green intensity in ONC212-treated HeLa cancer cells, implying insignificant $\Delta\Psi_m$ loss (Fig. S3a). Hence, despite of extensive caspase-3 cleavage and cell death observed at 48 h in ONC212-treated cancer cells, the loss in $\Delta\Psi_m$ was minimal. To further corroborate this data, we performed a simultaneous analysis of nuclear condensation by Hoechst staining and $\Delta\Psi_m$ by TMRM staining (Fig. 3b). Only a minute fraction of cells with extensively condensed nuclei reflected loss in $\Delta\Psi_m$ whereas the remaining cells did not show reduction in TMRM fluorescence suggesting no loss of $\Delta\Psi_m$. However, we observed massive mitochondrial fragmentation in ONC212-treated cancer cells stained with Mitotracker Red (Fig. S3b). Overall, these results clearly demonstrate that ONC212 treatment stimulates apoptosis independent of $\Delta\Psi_m$ loss.

To gain a deeper insight into MOMP, we next studied the release of cyt-c from mitochondria in HeLa and A549 cells after 48 h of treatment with ONC212 by immunofluorescence assay [40] (Fig. 3c). Strikingly, cyt-c release was not observed in ONC212-treated cancer cells as evidenced by granular pattern suggesting mitochondrial localization of cyt-c. Remarkably, despite no cyt-c release from mitochondria, we found several cells with condensed nuclei. Meanwhile, with the positive control etoposide treatment, many cells had a diffused pattern of cyt-c, indicating its release from mitochondria to the cytosol (data not shown). These findings provide strong evidence that ONC212 triggers caspase-3-mediated apoptosis independently of MOMP.

Bcl-2 and Bcl-xL inhibit ONC212-mediated apoptosis

The precise balance of pro- and anti-apoptotic Bcl-2 proteins regulates MOMP and subsequent caspase activation during apoptosis [41]. Antiapoptotic Bcl-2 proteins such as Bcl-2, Bcl-xL, etc. inhibit proapoptotic Bax and Bak proteins which are essentially required for MOMP [42, 43]. As ONC212 treatment failed to induce MOMP despite of the caspase-3-mediated apoptosis in cancer cells, we next investigated the expression of key Bcl-2 family proteins to understand their role in ONC212-mediated apoptosis. The expression of antiapoptotic Bcl-2 and Bcl-xL proteins was remarkably increased upon ONC212 treatment in a time-dependent manner in both the cell lines till 48 h (Fig. 4a, S4a and S4b). Whereas, the expression levels of proapoptotic Bax and Bak did not alter significantly. This upregulation of antiapoptotic Bcl-2 and Bcl-xL proteins may likely explain the limited MOMP in ONC212-treated cancer cell [41].

According to prior research, ONC212 inhibits mitochondrial respiration and hyperactivates the mitochondrial protease ClpP, which can lead to mitochondrial proteotoxicity [13, 19]. Consequently, we also examined the expression of TRAP1, a key mitochondrial chaperon protein for members of the HSP90 family. TRAP1 acts as a pro-survival factor by maintaining the integrity of mitochondria, activating the mitochondrial unfolded protein response, and shifting the cells from OXPHOS towards glycolysis to generate the cellular ATP [44, 45]. However, TRAP1 expression was not modulated in HeLa whereas it was upregulated in A549 cells upon ONC212 treatment (Fig. 4a and S4a). This cell-dependent variation in TRAP1 expression again ruled out the mitochondrial impairment as the primary and common cause for ONC212-induced apoptosis.

Despite insignificant MOMP and upregulation of antiapoptotic Bcl-2 family proteins, how ONC212 treatment potentially triggers caspase-mediated apoptosis remains an intriguing question. Several reports have highlighted that caspase-mediated cleavage of Bcl-2 and Bcl-xL can accelerate apoptosis rather than inhibit it [46, 47]. Focusing on this aspect, we further investigated whether overexpression of these survival proteins regulated ONC212-mediated apoptosis. In this regard, we generated Bcl-2 GFP and Bcl-xL GFP stably overexpressing HeLa and A549 cancer cells (Fig. S4c and d) and comparatively assessed apoptosis by examining nuclear condensation after treatment with ONC212. Bcl-2 GFP and Bcl-xL GFP overexpressing HeLa and A549 cells exhibited significantly lesser number of condensed nuclei when treated with ONC212 compared to HeLa and A549 cancer cells (Fig. S4e and f). Condensed nuclei were counted, plotted graphically and analysis showed significant statistical differences between the cells with and without Bcl-2/Bcl-xL GFP overexpression (Fig. 4b). To further confirm the data, we used flow cytometry with zombie stain to assess total cell death in ONC212-treated Bcl-2 GFP and Bcl-xL GFP overexpressing HeLa and A549 cell lines. As seen in Fig. 4c and Fig. S4g, the data show that

(See figure on next page.)

Fig. 4 ONC212 induces Bcl-2/Bcl-xL inhibitable apoptosis in HeLa and A549 cancer cells. **a.** Western blot images of Bcl-2 family proteins (Bcl-2, Bcl-xL, Bax, and Bak) and TRAP1 expression in control and ONC212 treated cells. Antiapoptotic Bcl-2 and Bcl-xL proteins were enhanced whereas proapoptotic Bax and Bak were slightly reduced by ONC212 treatment in cancer cells. **b.** The nuclear condensation was assessed under a fluorescence microscope by Hoechst staining after ONC212 treatment in wild-type and Bcl-2/Bcl-xL GFP overexpressing cancer cells (48 h). The Percentage of condensed nuclei in random fields represented graphically ($n = 3$, mean ± SEM), ** and *denotes $p < 0.01$ and $p < 0.05$ respectively in both control *vs* ONC212 treated groups. **c.** Flow cytometry histogram demonstrating comparative cell death after ONC212 treatment in wild type vs Bcl-2 GFP and Bcl-xL-GFP overexpressing HeLa and A549 cancer cells using zombie red staining

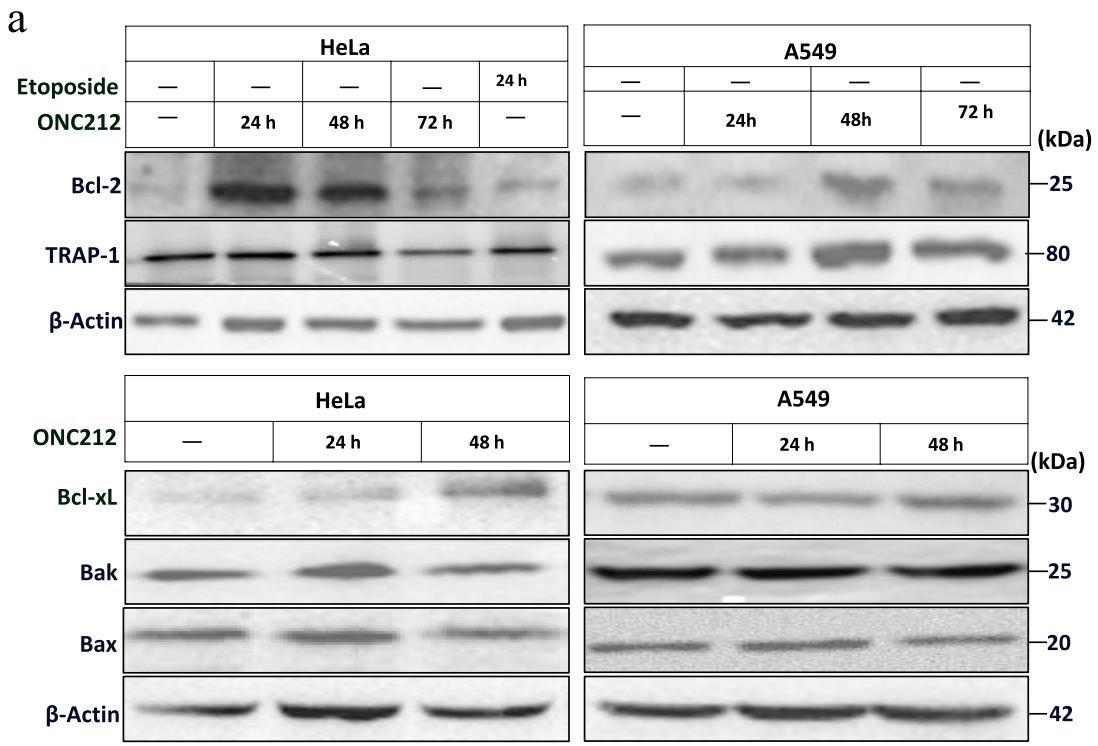

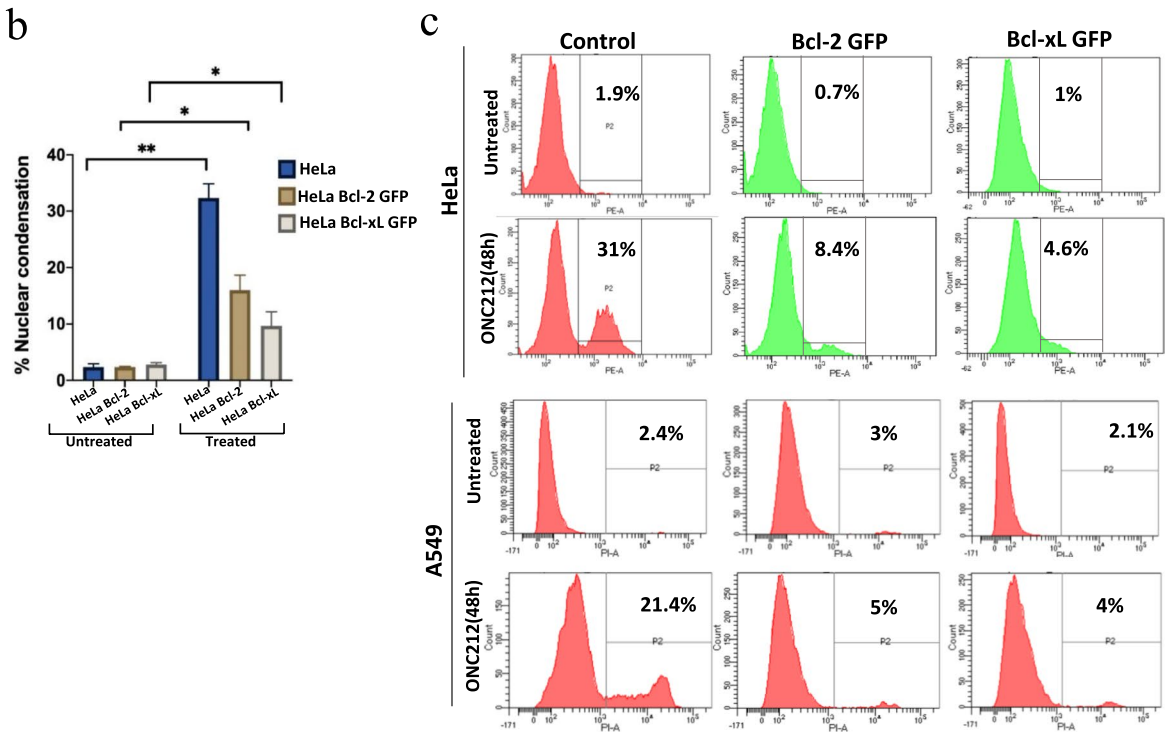

Fig. 4 (See legend on previous page.)

significantly lesser number of cells are undergoing apoptosis than non-transfected cancer cells. This reduced cell death in Bcl-2 GFP and Bcl-xL GFP overexpressing cancer cells indicate the cytoprotective role of Bcl-2/Bcl-xL proteins. Furthermore, we also observed upregulation of epithelial-mesenchymal transition (EMT) marker proteins (Snail, Vimentin, β-catenin) in ONC212-treated HeLa cells (Fig. S4h). These results indicate that Bcl-2/Bcl-xL upregulation might be conferring drug resistance against ONC212, as Bcl-2 overexpression is known to cause EMT-mediated drug resistance [48–50].

Navitoclax (ABT-263), a potent inhibitor of Bcl-2 and Bcl-xL, sensitized ONC212-mediated apoptosis

To overcome the drug-resistance mediated by Bcl-2/Bcl-xL upregulation upon ONC212 treatment, we adopted the drug combination strategy. In this regard, sub-lethal dose of Navitoclax, an inhibitor of Bcl-2 and Bcl-xL [51, 52], was selected based on MTT assays in HeLa and A549 cells (Fig. S5a and b). Accordingly, we treated the cells with ONC212 in the presence or absence of a sublethal dose of Navitoclax (0.25 μM in HeLa and 0.50 μM in A549) for a period of 24 h and evaluated its impact on cell death. Co-treatment with ONC212 and Navitoclax for 24 h significantly enhanced cell death in A549 and HeLa cancer cells compared to ONC212 alone at 24 or 48 h, as demonstrated by MTT assay (Fig. 5a and b), nuclear condensation assay (Fig. 5c and d), and Annexin-V/PI staining assay (Fig. 5e and S5c). Annexin-V/PI analysis showed a marked increase in both early (Annexin-V + /PI-) and late (Annexin-V + /PI +) apoptotic cell populations at 24 h upon treatment with the combination, hence proving co-treatment more effective than ONC212 alone. Consistent with these findings, western blot analysis of HeLa and A549 cells (Fig. 5f, g and S5d) revealed that the combination of ONC212 and Navitoclax resulted in substantially increased levels of cleaved caspase-3 and cleaved PARP, further validating the enhanced apoptotic response in both cell lines. It is worth mentioning that the amount of caspase-3 and PARP cleavage was remarkably higher after 24 h of ONC212 and Navitoclax combined treatment compared to 48 h of ONC212 treatment alone. These results indicate that inhibition of Bcl-2/Bcl-xL enhanced ONC212-mediated cell death via elevated caspase-3 activation.

As an agonist of mitochondrial protease ClpP, ONC212 is reported to impair the mitochondrial proteostasis which in turn, can induce mitochondrial chaperon proteins, especially HSPs such as HSP90 protein TRAP1 [13, 53]. To further verify the mitochondrial role in ONC212-mediated apoptosis, we examined the apoptosis in the presence of Tanespimycin (17-AAG), a potent small molecular inhibitor of HSP90 [54]. As shown by MTT and nuclear condensation assays (Fig. S5a, b, e, f and g) in HeLa and A549 cells, Tanespimycin is failed to modulate ONC212-induced apoptosis significantly, ruling out the participation of HSP90s, particularly mitochondrial TRAP-1.

Navitoclax potentiates ONC212-mediated caspase-3-dependent apoptosis independent of mitochondrial apoptotic events

Principally, being a Bcl-2/Bcl-xL inhibitor, Navitoclax when used in conjunction with ONC212 plausibly stimulate MOMP and cyt-c release and augment caspase-3 activation and apoptotic cell death. To delineate the mitochondrial apoptotic events, we analyzed $\Delta\Psi_m$ loss by TMRM staining (Fig. 6a) and cyt-c release by immunofluorescence in both HeLa and A549 cancer cell lines (Fig. 6 b and c). Interestingly and unexpectedly, we did not see significant $\Delta\Psi_m$ loss in cells treated with the combination of ONC212 and Navitoclax for 24 h, despite extensive caspase-3 activation and cell death at the same time point in previous results. Conversely, as the positive control, etoposide treatment revealed distinctive and drastic reduction in TMRM fluorescence intensity in HeLa and A549 cells when compared to untreated cells. Furthermore, despite mitochondrial fragmentation as seen by the granular pattern (Fig. 6b and c), we found no evidence of cyt-c release from mitochondria to cytosol following ONC212 treatment, whether Navitoclax was present or not. As seen in magnified images (Fig. 6b),

(See figure on next page.)

Fig. 5 Bcl-2/Bcl-xL inhibitor Navitoclax sensitizes ONC212-mediated apoptosis. **a** and **b.** MTT assay showing the comparative cell viability of HeLa and A549 cancer cells treated with ONC212 (24 h) in the presence and absence of Navitoclax (0.25 μM in HeLa and 0.50 μM in A549 for 24 h). **c** and **d.** Hoechst-stained fluorescence microscopic images demonstrate comparative nuclei condensation in HeLa and A549 cells induced by ONC212, Navitoclax and a combination of both. Arrows indicate condensed nuclei. The percentage of condensed nuclei in random fields is represented graphically ($n = 3$, mean ± SEM). **e.** Representative flow cytometry scatter plots illustrating Annexin V-FITC/PI staining in HeLa and A549 cell lines under various treatment conditions: control, ONC212 (24 h), ONC212 (48 h), and ONC212 + NAV (24 h). The combination of ONC212 with Navitoclax shows a substantial increase in the Annexin V-FITC positive population compared to ONC212 alone at 24 h or 48 h, indicating enhanced apoptosis. **f** and **g.** Western blot showing the cleavage of caspase-3 and PARP in HeLa and A549 cells on treatment with ONC212 in the presence and absence of Navitoclax. Etoposide is used as a positive control. Co-treatment with ONC212 and Navitoclax for 24 h synergistically enhanced caspase-3 and PARP cleavage compared to ONC212 treatment for 24 h and 48 h

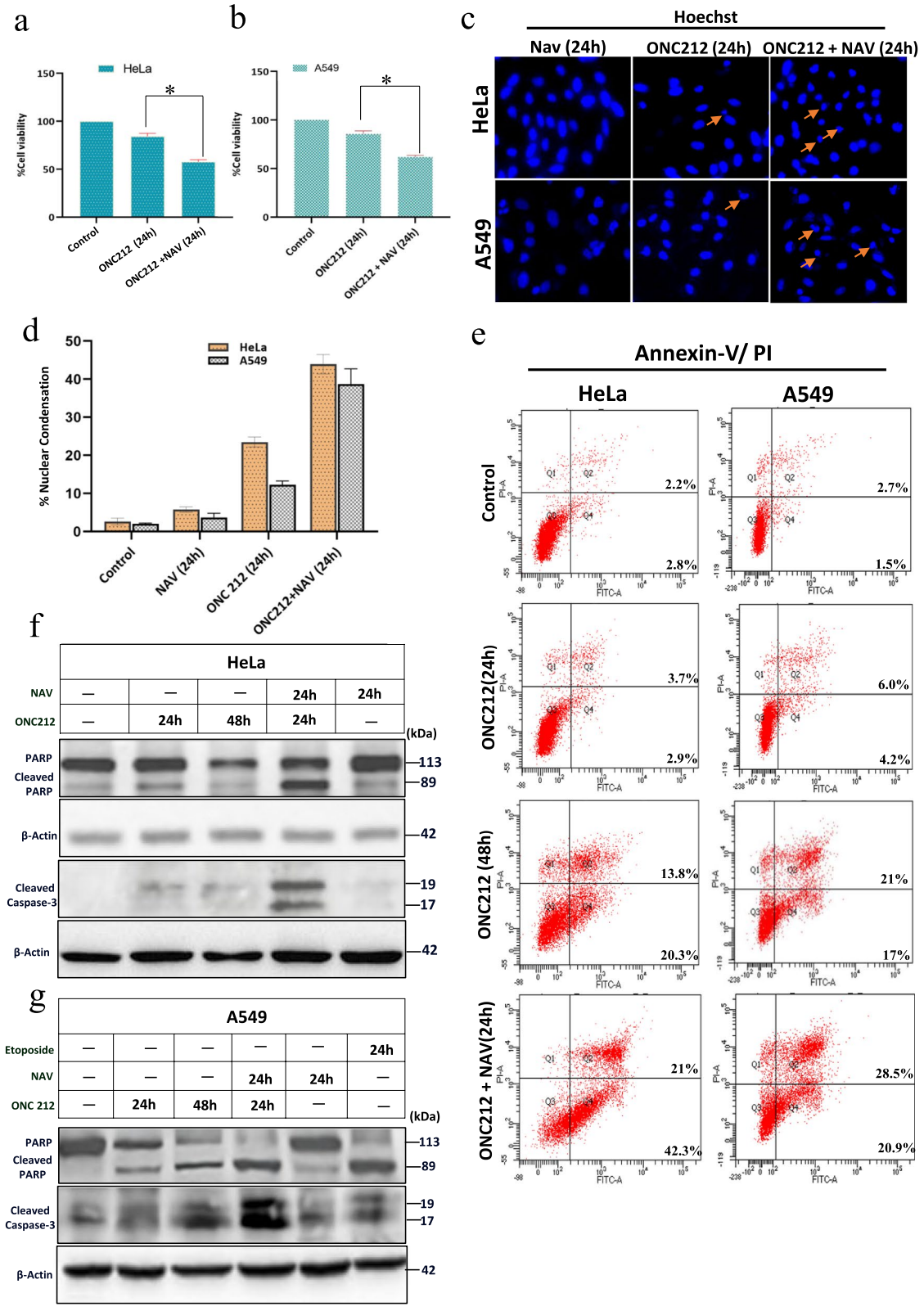

Fig. 5 (See legend on previous page.)

prominent granular pattern of cyt-c was visible in treated A549 cells despite of remarkable nuclear condensation indicating minimal cyt-c release from mitochondria.

To further verify these findings, we read out both $\Delta\Psi_m$ loss and cyt-c-GFP release simultaneously in HeLa cells stably expressing cyt-c-GFP under a fluorescence microscope. As seen in Fig. 6d, irrespective of the presence and absence of Navitoclax, ONC212 treatment failed to trigger effective $\Delta\Psi_m$ loss and cyt-c-GFP release in cancer cells. These results verify that even in the presence of Navitoclax, ONC212 did not significantly trigger crucial mitochondrial apoptotic events despite significant caspase-3 activation and cell death. To further substantiate our findings, we assessed the temporal kinetics of cyt-c-GFP release upon treatment with ONC212 and navitoclax in the presence of propidium iodide stain in HeLa cyt-c-GFP stable cells by confocal microscopy. The representative images of sequential time-lapse frames demonstrated temporal uptake of PI stain without the release of cyt-c-GFP from mitochondria (Fig S6a). To further corroborate this atypical observation, we performed end time-point imagining of different areas which again showed that, even in the late-apoptotic cells as marked by PI uptake, there is no substantial translocation of cyt-c-GFP from mitochondria to cytosol (Fig. 6e). These results indicate that caspase-3 activation occurred independent of MOMP and cyt-c release.

Caspase-3 activation primarily occurs via initiator caspase-9 which gets activated by MOMP and cyt-c release with the formation of apoptosome complex [34, 35, 55]. To further characterize the mitochondrial-independent unconventional caspase-3 activation, we evaluated the role of initiator caspase-9 in caspase-3 activation and cell death induced solely by ONC212 treatment as well as in combination with Navitoclax. Initially, we analyzed the cleavage of procaspase-9 by western blot in both HeLa and A549 cells treated with ONC212 as well as a combination of ONC212 and Navitoclax (Fig. 7a and S6b). As expected, there was no induction in caspase-9 cleavage reflected upon treatment with ONC212 and its combination with Navitoclax. Therefore, it again substantiates that MOMP, a central event of apoptosis does not have much role in cell death triggered by ONC212 alone or a combination of ONC212 with Navitoclax. Notably, the co-treatment of ONC212 and Navitoclax did not induce caspase-8 cleavage as well and thereby, eliminating contribution of extrinsic apoptotic pathway (Fig. S6c).

To further examine the role of caspase-9, comparative cell death was assessed by performing MTT assay in both Hela and A549 cancer cells with and without specific caspase-9 inhibitor Ac-LEHD-CMK. As seen in the Fig. 7b and c, rather than inhibiting cell death, ONC212 treatment sensitized cell death in the presence of Ac-LEHD-CMK. Similarly, upon treatment with ONC212 and Navitoclax combination, cell death was sensitized in the presence of caspase-9 inhibitor. On the other hand, Ac-LEHD-CMK presence drastically reduced the positive control etoposide-mediated cell death. To validate further, we examined the nuclear condensation in both the cells treated with the drugs in the presence and absence of Ac-LEHD-CMK (Fig. 7d and e). As shown in the graph (Fig. 7f and g), the presence of Ac-LEHD-CMK significantly augmented the condensed nuclei with the treatment of ONC212 and its combination with Navitoclax. Subsequently, to determine the caspase-3 activity in the presence and absence of caspase-9 inhibitor, we utilized HeLa cancer cells transiently expressing caspase-3 biosensor probe GC3AI (GFP-based, caspase-3-like, protease activity indicator). Principally, in the absence of caspase-3 activation, the probe remains in a locked dark state, whereas cleavage by caspase-3 activity results in fluorescence (Fig. 7h) [56–58]. To validate the functionality of the probe, cells were treated with etoposide and GFP fluorescence was visualized under a fluorescent microscope. As expected, the treated cells demonstrated enhanced GFP fluorescence whereas control cells showed imperceptible fluorescence (Fig. S6d). By employing flow cytometry, we subsequently read out the comparative fluorescence-based caspase-3 activity induced by ONC212 alone and its combination with Navitoclax in the presence and absence of Ac-LEHD-CMK (Fig. 7i). Similar to MTT results, we

(See figure on next page.)

Fig. 6 A combination of ONC212 and Navitoclax induced insignificant mitochondrial membrane potential ($\Delta\Psi_m$) loss and cytochrome c release in cancer cells. **a.** Flow cytometry histogram showing the relative fluorescence intensity of mitochondrial stain TMRM in cells treated with ONC212 (48 h), a combination of ONC212 and Navitoclax (24 h) and etoposide (positive control). **b** and **c**. Immunofluorescence images (A549: 60X and HeLa: 40X, scale bar: 50 µm) showing cytochrome c localization in control, ONC212 (48 h) and ONC212 with navitoclax treated (24 h) A549 and HeLa cancer cells. The magnified area highlights the granular pattern of cyt-c even in the A549 cell with condensed nuclei upon treatment suggesting insignificant cyt-c release from mitochondria to cytosol. **d.** Fluorescence images (20X, scale bar: 100 µm) of cyt-c-GFP stably expressing HeLa cells stained with mitochondrial TMRM dye after treatment. Insignificant alternation in TMRM intensity and GFP granular pattern suggest negligible $\Delta\Psi_m$ loss and cyt-c-GFP release after treatment. **e.** Confocal microscopic images of HeLa cyt-c-GFP cells stained with propidium iodide (PI) after 24 h of co-treatment with ONC212 and Navitoclax. (40X, scale bar:10 µm). Two different fields are shown. As shown by arrows, even PI positive cells reflected granular pattern of cyt-c-GFP indicating insignificant release of cyt-c-GFP in cytosol

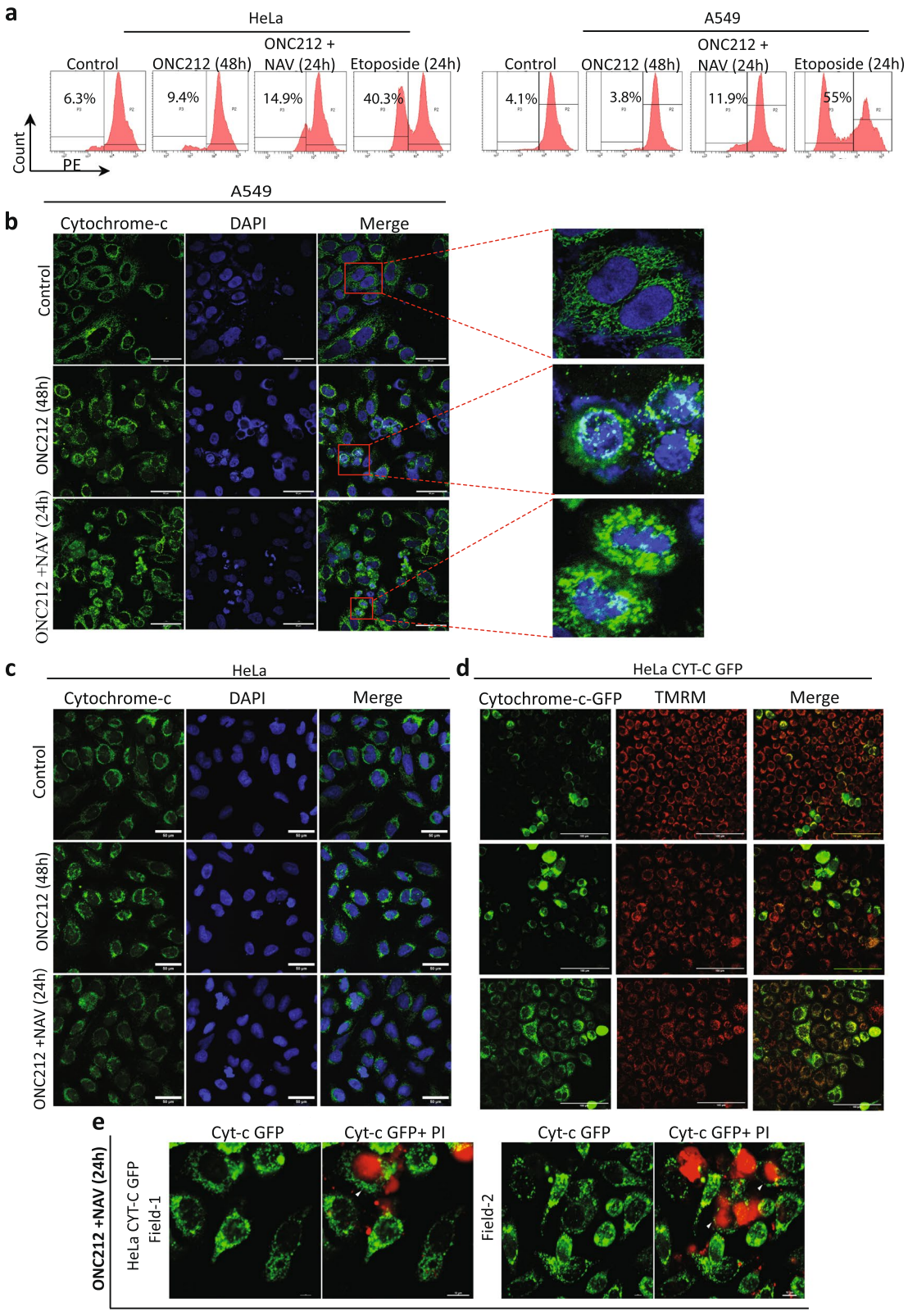

Fig. 6 (See legend on previous page.)

observed increased caspase-3 activity in the presence of Ac-LEHD-CMK by ONC212 as well as ONC212 and Navitoclax combination. Nevertheless, Ac-LEHD-CMK sharply attenuated caspase-3 activity in the presence of etoposide. These results clearly confirm that ONC212 alone and its combination with Navitoclax, both triggered caspase-3 mediated cell death independent of mitochondria and caspase-9 activation.

Discussion

ONC212 has received significant attention as a novel mitocan with potential anticancer activity. According to reports, ONC212 functions as an agonist of mitochondrial ClpP protease, impairing mitochondrial respiration, i.e., OXPHOS, and thereby leading to the death of many cancer cells [11–15, 58]. ONC212 has been also identified as the agonist of GPCR GPR132 which induces an integrated stress response culminating in death in cancer cells [14]. With multiple molecular targets, ONC212 has reflected broad-spectrum anticancer activity against various cancer cells. However, it also creates challenges to dissect the precise mechanism of cell death elicited by this potential compound.

In general, most of the anticancer drugs trigger apoptosis in cancer cells via intrinsic/mitochondrial pathways [33, 59]. Typically, in the mitochondrial apoptotic pathway, Bax and Bak proteins- mediated MOMP allows cyt-c release into cytosol and trigger caspase-9 activation via the formation of apoptosome complex. Subsequently, caspase-9 activates executioner caspase-3 which ultimately leads to cell death [3, 31, 34, 37, 39, 60]. As ONC212 targets the mitochondria of cancer cells, we expected it would induce MOMP and downstream apoptotic events. Unexpectedly, despite substantial activation of executioner caspase-3 and cell death in both HeLa and A549 cancer cells, ONC212 did not trigger MOMP as reflected by the lack of cyt-c release from mitochondria. Concurrently, we did not observe cleavage of caspase-9 and upregulation of Bax and Bak proteins. Therefore, ONC212-induced activation of caspase-3 independent of MOMP and cyt-c release.

Generally, apoptosis-induced MOMP is tightly coupled with the loss of $\Delta\Psi_m$, a key indicator of mitochondrial respiratory activity and ATP production [39]. Upon examination of $\Delta\Psi_m$ by both TMRM or JC-1 staining, we surprisingly did not observe substantial $\Delta\Psi_m$ loss as compared to the magnitude of cell death and caspase-3 activation even at 48 h of treatment. Simultaneous analysis of nuclear condensation with cyt-c and $\Delta\Psi_m$ showed that ONC212 triggered apoptosis independent of MOMP and $\Delta\Psi_m$ loss. The small percentage of $\Delta\Psi_m$ loss and imperceptible cyt-c release inevitably resulted from feedback amplification on mitochondria by activated caspase-3.

Caspase-3 can also be activated downstream by death receptor complex-mediated caspase-8 activation [37, 60]. Earlier studies have identified imipridones including ONC201 as activators of the TRAIL apoptotic pathway [16]. Therefore, we sought to determine if ONC212 treatment also induces cleavage of caspase-8. However, we found that ONC212 did not result in caspase-8 cleavage. Therefore, ONC212 treatment induced unconventional activation of caspase-3 independent of mitochondria or caspase-8 activation.

Previous reports suggested OXPHOS as the target of ONC212-mediated cell death. The cancer cells that rely on glycolysis undergo cell cycle arrest and upregulate glucose catabolism to resist apoptosis via prevention of ERK1/2 inhibition [61]. TRAP1, a HSP90-family mitochondrial chaperon is a known regulator of the metabolic switch of cancer cells towards glycolysis and mitochondrial adaptation [45]. However, TRAP1 expression was not varying in ONC212-treated HeLa cells whereas inhibition of TRAP1 by Tanespimycin did not escalate ONC212-mediated apoptosis in A549 cancer cells. All of these findings rule out mitochondria as the primary target of ONC212, albeit this may vary depending on the type of cancer cell.

Antiapoptotic Bcl-2 family proteins are known to maintain mitochondrial function by inhibiting MOMP and $\Delta\Psi_m$ loss [41]. It is noteworthy that the use of ONC212 in HeLa and A549 cells resulted in increased expression of Bcl-2 and Bcl-xL proteins. Despite its known antiapoptotic function, some studies have also shown that Bcl-2 can induce

(See figure on next page.)

Fig. 7 Cell Death induced by ONC212 alone or in conjunction with Navitoclax is augmented by caspase-9 inhibitor. **a.** Western blot showing the cleaved caspase-9 bands in HeLa and A549 cancer cells treated with ONC212 alone or its combination with Navitoclax. **b** and **c.** Percentage of cell viability is shown by MTT assay in HeLa and A549 cancer cells treated with the drugs in the presence and absence of caspase-9 inhibitor Ac-LEHD-CMK (50 μM). Etoposide is used as a positive control drug. ($n = 3$, mean ± SEM). **d, e, f** and **g.** Comparative nuclei condensation based on Hoechst-staining in HeLa and A549 cells treated with ONC212, Navitoclax and a combination of both, in the presence or absence of Ac-LEHD-CMK. The percentage of condensed nuclei in random fields is represented graphically ($n = 3$, mean ± SEM). **h.** A schematic diagram describing the functionality of GFP sensor caspase-3-like protease activity indicator (GC3AI) to monitor intracellular caspase-3 activity. Activated caspase-3 cleaves the DEVD linker sequence of the probe which in turn allows masked GFP to fluoresce. **i.** Flow cytometry scatter plot representing the fluorescence intensity of transiently expressing GC3AI in HeLa cells. Ac-LEHD-CMK enhanced the GFP fluorescence in ONC212 alone or in combination with ONC212 and Navitoclax-treated cells. Etoposide was used as the positive control

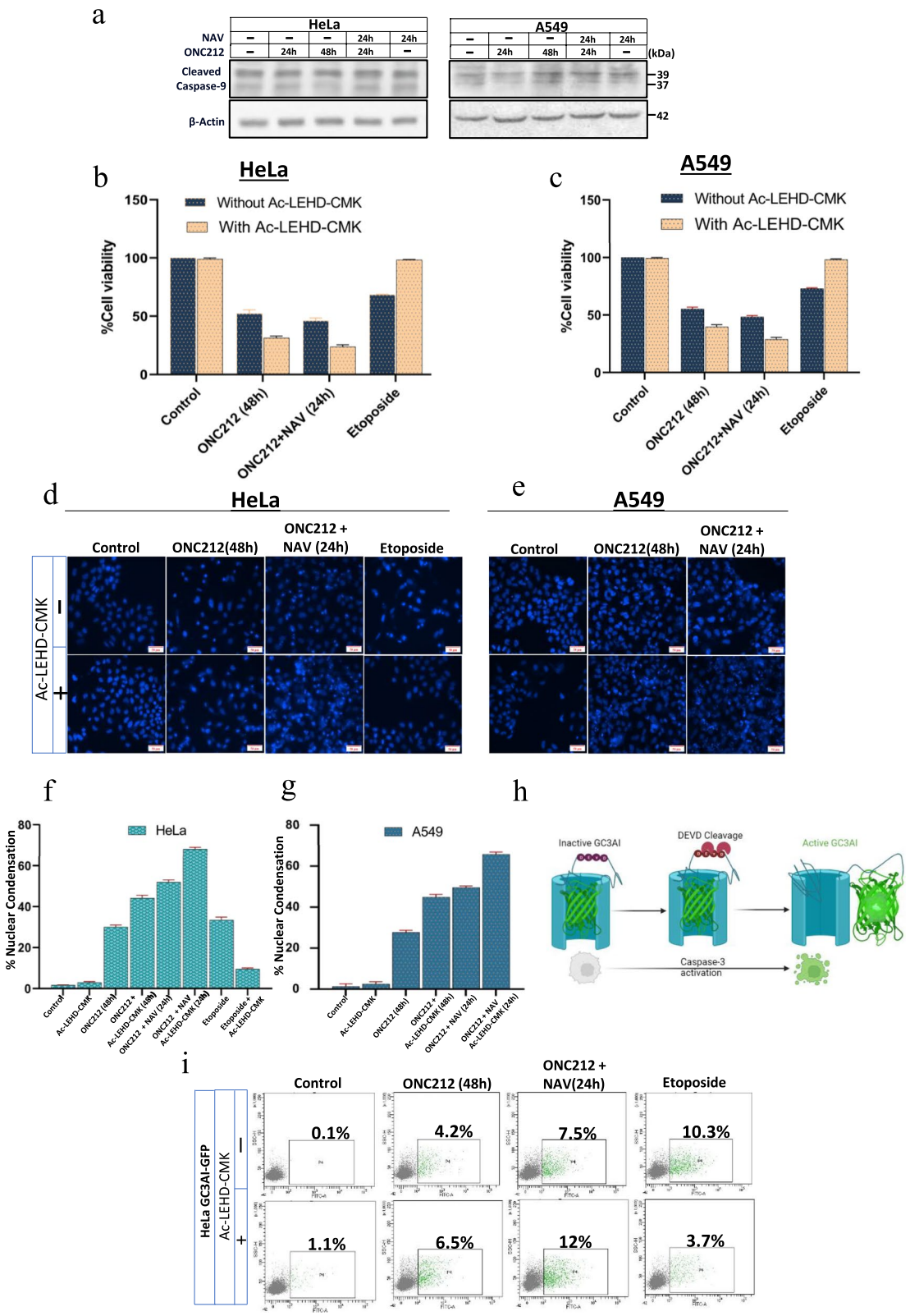

Fig. 7 (See legend on previous page.)

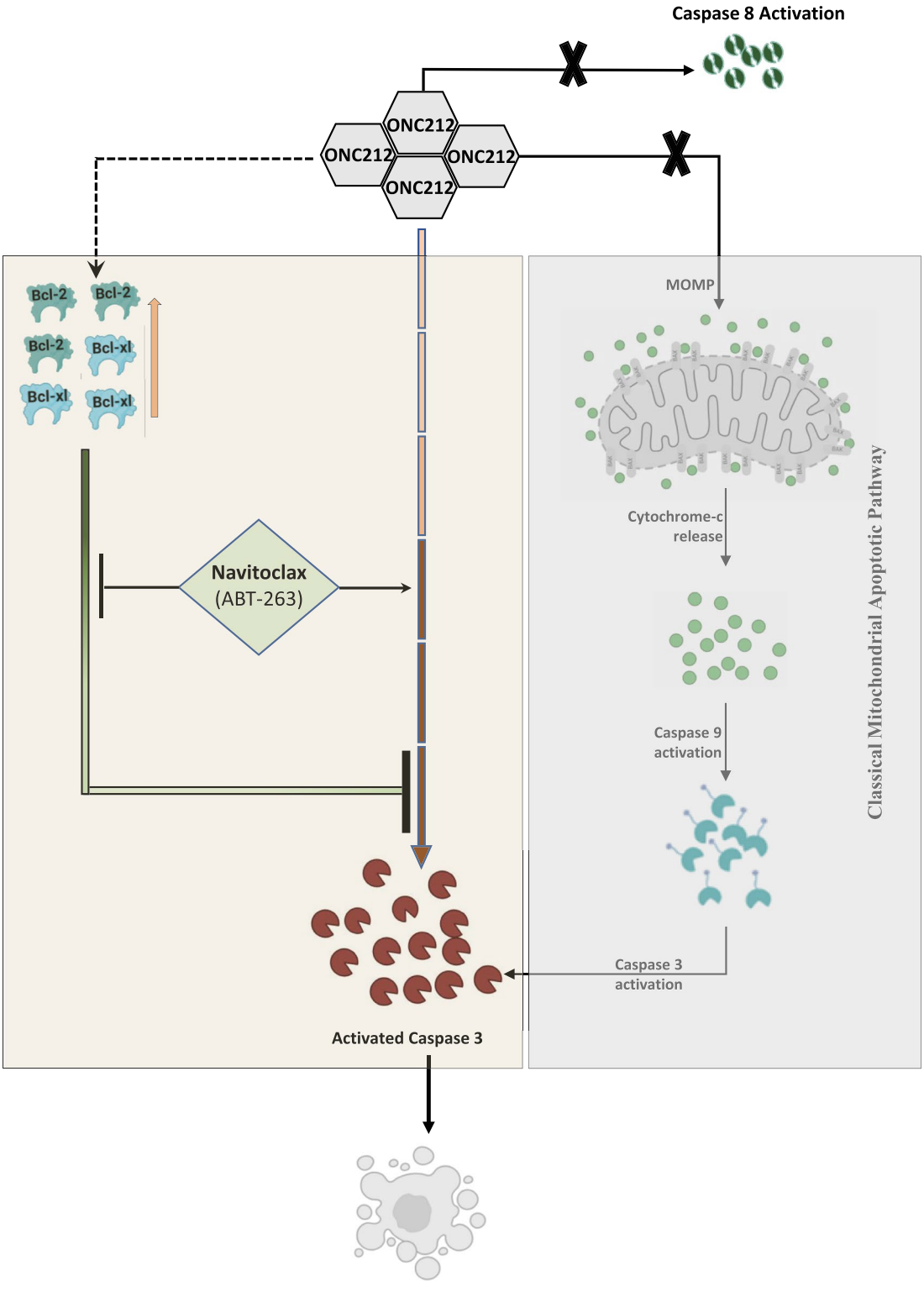

Fig. 8 A schematic diagram demonstrating ONC212 induced apoptosis signalling. ONC212 induces caspase-3 activation independently of cytochrome c release and caspase-8 activation, two key events in the intrinsic and extrinsic apoptosis signaling pathways respectively. This atypical caspase-3 activation is negatively regulated by Bcl-2 and Bcl-xL in the cell. Inhibition of these proteins with Navitoclax augments caspase-3 activity, dramatically sensitizing cells to ONC212-induced apoptosis

apoptosis upon its cleavage [46]. However, exogenous overexpression of these proteins was able to reduce ONC212-induced cell death effectively confirming their antiapoptotic function. Additionally, treatment with ONC212 in conjunction with a sublethal dose of the Bcl-2/Bcl-xL inhibitor Navitoclax (ABT-263) substantially sensitized cell death in HeLa and A549 cancer cells. This is consistent with a recent study that found a significant synergistic anti-leukaemia activity of ONC212 and a Bcl-2 inhibitor, ABT-199, in a MOLM-13 xenograft mice model [14].

Unexpectedly, despite the significantly increased caspase-3 cleavage and percentage of cell death by the combination of Navitoclax and ONC212 compared to ONC212 treatment alone, the extent of $\Delta\Psi_m$ loss and cyt-c release was still significantly lower than the percentage of cell death in co-treatment. Caspase-9 inhibition sensitized caspase-3 activation and cell death rather than decreasing it, actively ruling out a mitochondrial role. Apparently, the upregulation of Bcl-2 and Bcl-xL function as a cytoprotective drug-resistance mechanism induced by ONC212 treatment in cancer cells.

However, it would be fascinating to reveal how Bcl-2/Bcl-xL hinders ONC212-mediated mitochondrial-independent caspase-3 activation. How caspase-9 inhibitor sensitized ONC212 mediated mitochondrial independent caspase-3 activation and cell death, remains a puzzle to be resolved. In summary, ONC212 induces apoptosis through a non-canonical mechanism of caspase-3 activation that is independent of the mitochondria and the extrinsic death receptor pathway, yet inhibited by Bcl-2/Bcl-xL (Fig. 8).

Nevertheless, the upstream signal that causes caspase-3 activation in ONC212-mediated apoptosis in cancer cells remains an intriguing question. There have been reports of alternative ways for such atypical caspase-3 activation [62–65]. Antineoplastic agents such as PAC-1, for instance, are known to elicit direct caspase activation via zinc chelation [66, 67]. A few reports have also demonstrated that lysosomal proteases activate caspase-3 [68, 69]. Nevertheless, further systematic investigation is required to elucidate the likelihood of direct caspase-3 activation and a lysosomal role in ONC212-mediated apoptosis.

Most cancer cells harbour mutations or chromatin aberrations that impairs mitochondrial apoptotic cascades, leading to apoptosis resistance and treatment failure [2]. Therefore, mitochondrial-independent caspase-3-mediated cell death highlights the advantage of ONC212 as a promising and potential anticancer drug. ONC212 could act as a potent anticancer drug for tumors with defective mitochondrial apoptotic machinery such as altered expression or mutations in Bax/Bak, inactivation of Apaf-1, Caspase-9 deficiency, etc. It could also be utilized effectively in combination chemotherapy with Bcl-2/Bcl-xL inhibitors to treat tumors with high expression of Bcl-2 and Bcl-xL proteins.

Abbreviations

GFP	Green Fluorescent Protein
Bcl-2	B-cell Lymphoma 2
Bax	Bcl-2 Associated X Protein
MOMP	Mitochondrial Outer Membrane Permeabilization
Bak	Bcl-2 Antagonist/Killer 1
EMT	Epithelial Mesenchymal Transition
TMRM	Tetra Methyl Rhodamine Methyl ester
JC1	5,5,6,6′-Tetrachloro-1,1′,3,3′ tetraethylbenzimi-dazoylcarbocyanine iodide
GC3A1	(GFP-based, caspase-3-like, protease activity indicator)
TRAP1	Tumor necrosis factor receptor-associated protein 1
17-AAG	17-N-allylamino-17-demethoxygeldanamycin

Supplementary Information

The online version contains supplementary material available at https://doi.org/10.1186/s12964-024-01817-1.

Supplementary Material 1. Figure S1a and b: Bright field microscopy images 10X) of HeLa and A549 cancer cells with and without ONC212 treatment after 48 h. Figure S2a and b: Flow cytometric analysis of cell cycle stages in HeLa and A549 cancer cells upon ONC212 treatment: ONC212 treatment (24 h) increased the cell population in G1/G0 phase in both the cancer cells. Figure S2c: Densitometric analysis of Western blots for cleaved PARP, caspase-3, and caspase-8 in control and ONC212-treated A549 and HeLa cells at 24- and 48-h post-treatment using ImageJ (FIJI). Protein levels were normalized to β-actin and expressed as fold change relative to controls. *(n = 2)*. Figure S2d: Flow cytometry histograms showing comparative cell death in the presence and absence of pan-caspase inhibitor (Z-VAD-FMK) assessed via zombie red staining of cells after ONC212 treatment. Only dead cells are permeable to amine-reacting zombie red stain. Figure S3a: Mitochondrial membrane potential ($\Delta\Psi_m$) loss was analysed by staining control and ONC212 treated HeLa cancer cells with JC1 dye. As seen in fluorescent microscopy images (scale bar: 50 µm), even upon ONC212 treatment, JC1 did not convert significantly in its monomeric (green) form and remains as aggregates (Orange). Figure S3b: Fluorescent microscopic images of HeLa cancer cells stained with Mitotracker Red: As shown in zoomed images, ONC212 treatment caused extensive mitochondrial fragmentation (granular pattern) when compared to untreated cells. Figure S4a and b: Densitometric analysis of western blots for Bcl-2, Bcl-xL, Bax, Bak and TRAP1 in control and ONC212-treated HeLa and A549 cells at various timepoints using ImageJ (FIJI). Protein levels were normalized to β-actin and expressed as fold change relative to control. *(n = 2)*. Figure S4c and d: Western blot showed the overexpression of Bcl-2-GFP and Bcl-xL-GFP in HeLa and A549 cancer cells. Both, the endogenous protein bands and GFP fusion protein bands are visible as the probing was performed with antibodies against Bcl-2 and Bcl-xL. Figure S4e and f: Hoechst-stained fluorescence microscopic images showing the comparative nuclei condensation induced by ONC212 in wild type verses Bcl-2-GFP and Bcl-xL-GFP overexpressing HeLa and A549 cancer cells. Figure S4g: The percentage of zombie positive cells (dead cells) are represented graphically for control, Bcl-2 and Bcl-xL overexpressing HeLa cancer cells ($n = 3$, mean ± SEM). Figure S4h: Western blot demonstrate the upregulation of EMT marker proteins upon ONC212 treatment (24 h) in HeLa cancer cells. Figure S5a and b: MTT assay showing percentage of cell viability in HeLa and A549 cancer cells treated with different doses of Navitoclax (solid line) or Tanespimycin (dotted line) for 24 h. Figure S5c: HeLa and A549 cells were treated with ONC212 alone or in combination with Navitoclax (Bcl-2/Bcl-xL inhibitor) for 24 h. Apoptosis was quantified by Annexin V-FITC/PI staining. Bars represent the percentage of apoptotic (Annexin V + /PI- & Annexin V + /PI +) cells. Data shown are mean ± SEM from three independent experiments. ** denotes $p < 0.01$, ***denotes $p < 0.001$ compared to ONC212 alone for 24 h. Figure S5d: Western blot of caspase-3 and cleaved PARP in HeLa and A549 cells treated with ONC212 alone or combined with Navitoclax were quantified using ImageJ (FIJI). Samples from multiple timepoints were analyzed with normalization of protein levels to β-actin and expressed as fold change relative to untreated controls. *(n = 2)*. Figure S5e: MTT assay showing the cell viability percentages in HeLa and A549 cancer cells treated with ONC212 alone

or with Tanespimycin (0.25 μM in HeLa and 0.50 μM in A549) for 24 h. Presence of Tanespimycin did not alter ONC212 mediated cell death significantly. Figure S5f and g: Hoechst-stained fluorescence microscopic images showing nuclei condensation induced by ONC212 in HeLa and A549 cells in the presence and absence of Tanespimycin. The condensed nuclei were counted from three random images and plotted graphically to represent percentage of nuclear condensation. ($n = 3$, mean ± SEM). Figure S6a: Confocal microscopic images of HeLa cyt-c-GFP stained with PI and co-treated with ONC212 and Navitoclax. Time -lapse kinetics of cyt-c release and PI uptake is shown at different time points treatment. (40X, scale bar: 20 μm). Figure S6b: Densitometric analysis of western blots for cleaved caspase-9 in control and ONC212 alone or in combination with Navitoclax treated HeLa and A549 cells at various timepoints using ImageJ (FIJI). Protein levels were normalized to β-actin and expressed as fold change relative to control. *($n = 2$)*. Figure S6c: Western blot of caspase-8 in HeLa cells. Figure S6d: Fluorescent and bright field microscopic images of HeLa cells transiently expressing GFP based caspase-3 sensor probe GC3AI. Etoposide (20 μM, 24 h) treatment potentially enhanced the GFP fluorescence suggesting induction of caspase-3 activity.

Acknowledgements
Author M. Seervi is pleased to acknowledge SERB CRG grant (CRG/2020/002009) funded by Department of Science and Technology, Government of India and AIIMS early career intramural research grant (A-830) for the financial support. We thank Head, Department of Biochemistry, AIIMS, New Delhi for microscope facility, Flow-cytometer facility (CCRF, AIIMS, New Delhi) and Dr. T. R. Santhosh Kumar, RGCB, Trivandrum for gifting HeLa cyt-c-GFP cells.

Authors' contributions
‡ These authors contributed equally: Vishal Basu, Shabnam. Experimental conception, design, analysis and manuscript preparation were performed by MS and VB. VB and S performed most of the experiments and data arrangement. YM, SS and MA assisted in few initial experiments and BKV gave intellectual inputs.

Availability of data and materials
No datasets were generated or analysed during the current study.

Declarations

Competing interests
The authors declare no competing interests.

Received: 18 January 2024 Accepted: 4 September 2024
Published online: 13 September 2024

References

1. Warburg O. On the Origin of Cancer Cells. Science. 1956;123:309–14.
2. Hanahan D. Hallmarks of Cancer: New Dimensions. Cancer Discov. 2022;12:31–46.
3. Green DR, Reed JC. Mitochondria and Apoptosis. Science. 1998;281:1309–12.
4. Dong L, Gopalan V, Holland O, Neuzil J. Mitocans Revisited: Mitochondrial Targeting as Efficient Anti-Cancer Therapy. Int J Mol Sci. 2020;21:7941.
5. Boukalova S, Rohlenova K, Rohlena J, Neuzil J. Mitocans: Mitochondrially Targeted Anti-cancer Drugs. Mitochondrial Biology and Experimental Therapeutics. 2018. p. 613–35.
6. Neuzil J, Dong L-F, Rohlena J, Truksa J, Ralph SJ. Classification of mitocans, anti-cancer drugs acting on mitochondria. Mitochondrion. 2013;13:199–208.
7. Bonner ER, Waszak SM, Grotzer MA, Mueller S, Nazarian J. Mechanisms of imipridones in targeting mitochondrial metabolism in cancer cells. Neuro Oncol. 2021;23:542–56.
8. Przystal JM, Cianciolo Cosentino C, Yadavilli S, Zhang J, Laternser S, Bonner ER, et al. Imipridones affect tumor bioenergetics and promote cell lineage differentiation in diffuse midline gliomas. Neuro Oncol. 2022;24:1438–51.
9. Chi AS. Identification of more potent imipridones, a new class of anti-cancer agents. Cell Cycle. 2017;16:1566–7.
10. Rizwan N, Shen Y, Iwanowicz E, Mulligan SP, Crassini KR, Christopherson R, et al. ONC-212 (I-39), a Novel Inhibitor of the UPR, Is Cytotoxic and Cytostatic Against CLL Cells Under in Vitro Conditions That Mimic the Tumor Microenvironment. Blood. 2018;132(Supplement 1):3145–3145.
11. Ferrarini I, Louie A, Zhou L, El-Deiry WS. ONC212 is a Novel Mitocan Acting Synergistically with Glycolysis Inhibition in Pancreatic Cancer. Mol Cancer Ther. 2021;20:1572–83.
12. Wagner J, Kline CL, Ralff MD, Lev A, Lulla A, Zhou L, et al. Preclinical evaluation of the imipridone family, analogs of clinical stage anti-cancer small molecule ONC201, reveals potent anti-cancer effects of ONC212. Cell Cycle. 2017;16:1790–9.
13. Lev A, Lulla AR, Wagner J, Ralff MD, Kiehl JB, Zhou Y, et al. Anti-pancreatic cancer activity of ONC212 involves the unfolded protein response (UPR) and is reduced by IGF1-R and GRP78/BIP. Oncotarget. 2017;8:81776–93.
14. Nii T, Prabhu VV, Ruvolo V, Madhukar N, Zhao R, Mu H, et al. Imipridone ONC212 activates orphan G protein-coupled receptor GPR132 and integrated stress response in acute myeloid leukemia. Leukemia. 2019;33:2805–16.
15. Raufi AG, Parker C, Zhou L, Prabhu VV, Allen J, El-Deiry WS. Abstract 1006: Combination therapy with MEK inhibitors and a novel anti-neoplastic drug, imipridone ONC212, demonstrates synergy in pancreatic ductal adenocarcinoma cell lines. Cancer Res. 2021;81:1006–1006.
16. Kline CL, Lulla AR, Dicker D, Allen JE, El-Deiry W. Abstract 2942: TRAIL pathway inducer ONC201/TIC10 primes multiple myeloma cells (MM) for apoptosis by downregulating X-linked inhibitor of apoptosis. Cancer Res. 2015;75:2942–2942.
17. Wang S, Dougan DA. The Direct Molecular Target for Imipridone ONC201 Is Finally Established. Cancer Cell. 2019;35:707–8.
18. Graves PR, Aponte-Collazo LJ, Fennell EMJ, Graves AC, Hale AE, Dicheva N, et al. Mitochondrial Protease ClpP is a Target for the Anticancer Compounds ONC201 and Related Analogues. ACS Chem Biol. 2019;14:1020–9.
19. Cole A, Wang Z, Coyaud E, Voisin V, Gronda M, Jitkova Y, et al. Inhibition of the Mitochondrial Protease ClpP as a Therapeutic Strategy for Human Acute Myeloid Leukemia. Cancer Cell. 2015;27:864–76.
20. Haynes CM, Petrova K, Benedetti C, Yang Y, Ron D. ClpP Mediates Activation of a Mitochondrial Unfolded Protein Response in C. elegans. Dev Cell. 2007;13:467–80.
21. Jacques S, van der Sloot AM, Huard CC, Coulombe-Huntington J, Tsao S, Tollis S, et al. Imipridone anticancer compounds ectopically activate the clpp protease and represent a new scaffold for antibiotic development. Genetics. 2020;214:1103–20.
22. Carter JL, Hege K, Kalpage HA, Edwards H, Hüttemann M, Taub JW, et al. Targeting mitochondrial respiration for the treatment of acute myeloid leukemia. Biochem Pharmacol. 2020;182:114253–114253.
23. Nguyen TTT, Shang E, Schiffgens S, Torrini C, Shu C, Akman HO, et al. Induction of Synthetic Lethality by Activation of Mitochondrial ClpP and Inhibition of HDAC1/2 in Glioblastoma. Clin Cancer Res. 2022;28:1881–95.
24. Aminzadeh-Gohari S, Weber DD, Catalano L, Feichtinger RG, Kofler B, Lang R. Targeting Mitochondria in Melanoma Biomolecules. 2020;10:1395.
25. Medema JP. Cancer stem cells: The challenges ahead. Nat Cell Biol. 2013;15:338–44.
26. Ayob AZ, Ramasamy TS. Cancer stem cells as key drivers of tumour progression. J Biomed Sci. 2018;25:20–20.
27. Seervi M, Rani A, Sharma AK, Santhosh Kumar TR. ROS mediated ER stress induces Bax-Bak dependent and independent apoptosis in response to Thioridazine. Biomed Pharmacother. 2018;106:200–9.
28. Rashmi R, Santhosh Kumar TR, Karunagaran D. Human colon cancer cells differ in their sensitivity to curcumin-induced apoptosis and heat shock protects them by inhibiting the release of apoptosis-inducing factor and caspases. FEBS Lett. 2003;538:19–24.
29. Martinez MM, Reif RD, Pappas D. Detection of apoptosis: A review of conventional and novel techniques. Anal Methods. 2010;2:996.

30. Eray M, Mikko M, Kaartinen M, Andersson LC, Pelkonen J. Flow cytometric analysis of apoptotic subpopulations with a combination of Annexin V-FITC, propidium iodide, and SYTO 17. Cytometry. 2001;43:134–42.
31. Elmore S. Apoptosis: a review of programmed cell death. Toxicol Pathol. 2007;35:495–516.
32. Gysin S, Lee S-H, Dean NM, McMahon M. Pharmacologic Inhibition of RAF→MEK→ERK Signaling Elicits Pancreatic Cancer Cell Cycle Arrest Through Induced Expression of p27Kip1. Cancer Res. 2005;65:4870–80.
33. Ripani P, Delp J, Bode K, Delgado ME, Dietrich L, Betzler VM, et al. Thiazolides promote G1 cell cycle arrest in colorectal cancer cells by targeting the mitochondrial respiratory chain. Oncogene. 2019;39:2345–57.
34. Green DR. The Mitochondrial Pathway of Apoptosis: Part I: MOMP and Beyond. Cold Spring Harb Perspect Biol. 2022;14:a041038.
35. Green DR. Caspase Activation and Inhibition. Cold Spring Harb Perspect Biol. 2022;14:a041020.
36. Chaitanya GV, Steven AJ, Babu PP. PARP-1 cleavage fragments: signatures of cell-death proteases in neurodegeneration. Cell Commun Signal. 2010;8:31–31.
37. Green DR. The Death Receptor Pathway of Apoptosis. Cold Spring Harb Perspect Biol. 2022;14:a041053.
38. Ricci J-E, Muñoz-Pinedo C, Fitzgerald P, Bailly-Maitre B, Perkins GA, Yadava N, et al. Disruption of Mitochondrial Function during Apoptosis Is Mediated by Caspase Cleavage of the p75 Subunit of Complex I of the Electron Transport Chain. Cell. 2004;117:773–86.
39. Tait SWG, Green DR. Mitochondria and cell death: outer membrane permeabilization and beyond. Nat Rev Mol Cell Biol. 2010;11:621–32.
40. Goldstein JC, Waterhouse NJ, Juin P, Evan GI, Green DR. The coordinate release of cytochrome c during apoptosis is rapid, complete and kinetically invariant. Nat Cell Biol. 2000;2:156–62.
41. Chipuk JE, Moldoveanu T, Llambi F, Parsons MJ, Green DR. The BCL-2 family reunion. Mol Cell. 2010;37:299–310.
42. Gavathiotis E, Suzuki M, Davis ML, Pitter K, Bird GH, Katz SG, et al. BAX Activation is Initiated at a Novel Interaction Site. 2008.
43. Dewson G, Kratina T, Czabotar P, Day CL, Adams JM, Kluck RM. Bak Activation for Apoptosis Involves Oligomerization of Dimers via Their α6 Helices. Mol Cell. 2009;36:696–703.
44. Altieri DC, Stein GS, Lian JB, Languino LR. TRAP-1, the mitochondrial Hsp90. Biochim Biophys Acta. 2012;1823:767–73.
45. Dharaskar SP, Amere SS. The mitochondrial chaperone TRAP-1 regulates the glutamine metabolism in tumor cells. Mitochondrion. 2023;69:159–70.
46. Lei X, Chen Y, Du G, Yu W, Wang X, Qu H, et al. Gossypol induces Bax/Bak-independent activation of apoptosis and cytochrome c release via a conformational change in Bcl-2. FASEB J. 2006;20:2147–9.
47. Lin B, Kolluri SK, Lin F, Liu W, Han Y-H, Cao X, et al. Conversion of Bcl-2 from Protector to Killer by Interaction with Nuclear Orphan Receptor Nur77/TR3. Cell. 2004;116:527–40.
48. Zuo J, Ishikawa T, Boutros S, Xiao Z, Humtsoe JO, Kramer RH. Bcl-2 Overexpression Induces a Partial Epithelial to Mesenchymal Transition and Promotes Squamous Carcinoma Cell Invasion and Metastasis. Mol Cancer Res. 2010;8:170–82.
49. Choi S, Chen Z, Tang LH, Fang Y, Shin SJ, Panarelli NC, et al. Bcl-xL promotes metastasis independent of its anti-apoptotic activity. Nat Commun. 2016;7:10384–10384.
50. Zhou P, Li B, Liu F, Zhang M, Wang Q, Liu Y, et al. The epithelial to mesenchymal transition (EMT) and cancer stem cells: implication for treatment resistance in pancreatic cancer. Mol Cancer. 2017;16:52–52.
51. Chen J, Jin S, Abraham V, Huang X, Liu B, Mitten MJ, et al. The Bcl-2/Bcl-XL/Bcl-w Inhibitor, Navitoclax, Enhances the Activity of Chemotherapeutic Agents In Vitro and In Vivo. Mol Cancer Ther. 2011;10:2340–9.
52. Tse C, Shoemaker AR, Adickes J, Anderson MG, Chen J, Jin S, et al. ABT-263: A Potent and Orally Bioavailable Bcl-2 Family Inhibitor. Cancer Res. 2008;68:3421–8.
53. Ishizawa J, Zarabi SF, Davis RE, Halgas O, Nii T, Jitkova Y, et al. Mitochondrial ClpP-Mediated Proteolysis Induces Selective Cancer Cell Lethality. Cancer Cell. 2019;35:721–37.e9.
54. Usmani S, Bona R, Li Z. 17 AAG for HSP90 Inhibition in Cancer – From Bench to Bedside. Curr Mol Med. 2009;9:654–64.
55. Rodriguez J, Lazebnik Y. Caspase-9 and APAF-1 form an active holoenzyme. Genes Dev. 1999;13:3179–84.
56. Zhang J, Wang X, Cui W, Wang W, Zhang H, Liu L, et al. Visualization of caspase-3-like activity in cells using a genetically encoded fluorescent biosensor activated by protein cleavage. Nat Commun. 2013;4:2157.
57. Moldovan C, Onaciu A, Toma V, Munteanu RA, Gulei D, Moldovan AI, et al. Current trends in luminescence-based assessment of apoptosis. RSC Adv. 2023;13:31641–58.
58. Nii T, Ishizawa J, Zhao R, Zeng J, Chachad D, Kojima K, et al. ONC212 Is a Potent Member of the Imipridone Class of Anti-Cancer Compounds That Induces p53-Independent Apoptosis in Hematological Malignancies. Blood. 2016;128:4059–4059.
59. Green DR. Cell Death and Cancer. Cold Spring Harb Perspect Biol. 2022;14:a041103.
60. Ashkenazi A, Dixit VM. Death Receptors: Signaling and Modulation. Science. 1998;281:1305–8.
61. Ley R, Balmanno K, Hadfield K, Weston C, Cook SJ. Activation of the ERK1/2 Signaling Pathway Promotes Phosphorylation and Proteasome-dependent Degradation of the BH3-only Protein. Bim J Biol Chem. 2003;278:18811–6.
62. Holinger EP, Chittenden T, Lutz RJ. Bak BH3 Peptides Antagonize Bcl-xL Function and Induce Apoptosis through Cytochrome c-independent Activation of Caspases. J Biol Chem. 1999;274:13298–304.
63. Chen T, Pengetnze Y, Taylor CC. Src inhibition enhances paclitaxel cytotoxicity in ovarian cancer cells by caspase-9-independent activation of caspase-3. Mol Cancer Ther. 2005;4:217–24.
64. Kitagawa H, Tani E, Ikemoto H, Ozaki I, Nakano A, Omura S. Proteasome inhibitors induce mitochondria-independent apoptosis in human glioma cells. FEBS Lett. 1999;443:181–6.
65. Nopp A, Lundahl J, Stridh H. Caspase activation in the absence of mitochondrial changes in granulocyte apoptosis. Clin Exp Immunol. 2002;128:267–74.
66. Peterson QP, Goode DR, West DC, Ramsey KN, Lee JJY, Hergenrother PJ. PAC-1 activates procaspase-3 in vitro through relief of zinc-mediated inhibition. J Mol Biol. 2009;388:144–58.
67. Seervi M, Joseph J, Sobhan PK, Bhavya BC, Santhoshkumar TR. Essential requirement of cytochrome c release for caspase activation by procaspase-activating compound defined by cellular models. Cell Death Dis. 2011;2:e207–e207.
68. Guicciardi ME, Leist M, Gores GJ. Lysosomes in cell death. Oncogene. 2004;23:2881–90.
69. Aits S, Jäättelä M. Lysosomal cell death at a glance. J Cell Sci. 2013;126:1905–12.

Publisher's Note